

# TaDA: Calibrated Probe Gating for Task-Domain LoRA Merging

Huy Quoc To<sup>1</sup>, Fuyi Li<sup>2</sup>, Guangyan Huang<sup>1</sup>, and Ming Liu<sup>1</sup>

<sup>1</sup> Deakin University, Melbourne, VIC, Australia

<sup>2</sup> Adelaide University, Adelaide, SA, Australia

{q.to, guangyan.huang, m.liu}@deakin.edu.au, fuyi.li@adelaide.edu.au

**Abstract.** Combining a task LoRA adapter with a domain LoRA adapter into a single unified model is a practical yet largely unexplored challenge. Existing methods treat both adapters as symmetric peers, applying uniform weights across all layers. We argue that task and domain adapters exhibit a consistent depth-dependent asymmetry across transformer architectures. Domain dominance increases with layer depth, while shallower layers retain stronger task-relevant signals. Motivated by this observation, we propose **TaDA** (**T**ask-**D**omain LoRA Merging), a training-free algorithm that exploits this structure through calibrated probe-guided per-layer gating and per-component subspace-aware merging. The gating assigns individual weights per layer and projection type using a probe signal proved invariant to adapter weight magnitude. The merging discards conflicting singular directions before combining the remaining components. **TaDA** produces a standard rank- $r$  LoRA adapter with zero inference overhead. On six scientific QA benchmarks with Llama-2-7B, TaDA achieves an average accuracy of 0.452, outperforming DARE-TIES by +3.6 percentage points and obtaining the best result on all six benchmarks. On six image classification benchmarks with ViT-L/16, TaDA reaches 85.9% average accuracy, improving over the strongest merging baseline while leading in three of the six individual benchmarks.

**Keywords:** LoRA merging · parameter-efficient fine-tuning · vision transformers · adapter composition

## 1 Introduction

The ecosystem of Low-Rank Adaptation (LoRA) adapters [10] has grown rapidly: model hubs now host thousands of adapters, each specializing in either a *task* (e.g. instruction following) or a *domain* (e.g. biomedical text, satellite imagery). Merging a task adapter and a domain adapter into a single unified adapter capable of answering domain-specific queries without retraining is a practical challenge. However, it remains largely unexplored. Existing merging methods [21, 22, 25] combine adapter weights uniformly at every layer, treating task and domain adapters as symmetric peers. However, we discover an interesting asymmetry. The task and domain adapters activate differently across transformer depth, and exploiting this structure leads to substantially better merges.

*A diagnostic finding.* By passing  $N=32$  domain-specific inputs through both adapters and measuring their activation norms at each layer, we find a consistent structural pattern across both language (Llama-2-7b) and vision (ViT-L/16) transformers. The domain dominance increases with depth. Shallower layers retain more task-relevant signal, while deeper layers are more strongly domain-dominant. However, measuring raw activation norms directly is unreliable. The norms grow with training duration rather than domain relevance. We address this with **calibrated probe scoring**. The domain relevance at each layer is computed as the ratio of activations on domain-specific inputs to activations on general inputs. We prove that this ratio is invariant to adapter weight magnitude. Uniform merging ignores this structure entirely. Assigning the same weight at every layer gives the domain adapter too much influence in shallower layers, degrading task format, and too little in deeper layers, diluting domain knowledge.

In this paper, we propose **TaDA** (**T**ask-**D**omain LoRA Merging), a training-free merging algorithm with two novelties. First, **calibrated probe-guided gating** computes a per-layer, per-module task weight using the calibrated score, with a module-type-aware threshold  $\tau_m$  that keeps output projections task-dominant to preserve answer format. Second, **per-component subspace-aware merging** decomposes both adapters via SVD, discards singular components whose directions conflict in both input and output feature spaces, and merges the remainder with individual per-component weights. The merged adapter is a standard rank- $r$  LoRA with zero inference overhead.

On six scientific text QA benchmarks using the Llama-2-7b backbone, **TaDA** achieves an average accuracy of 0.452, outperforming DARE-TIES by +3.6pp. It achieves the best results on all six benchmarks, including MMLU-CS. On six image classification benchmarks using ViT-L/16, TaDA achieves an average accuracy of 85.9%, outperforming all baselines including DARE-TIES (85.6%), while leading on three of the six individual benchmarks.

*Our contributions are:*

- We propose a novel merging algorithm for LoRA-based adapters. TaDA is a training-free merging algorithm that exploits the depth-dependent activation asymmetry between task and domain adapters via calibrated probe-guided per-layer gating and per-component subspace-aware filtering. Across both language and vision settings, TaDA achieves the best average performance among merging methods while preserving the standard rank- $r$  LoRA form and adding no inference-time overhead.
- We provide a systematic task  $\times$  domain merging benchmark spanning six scientific text QA benchmarks using Llama-2-7b and six image classification benchmarks using ViT-L/16. Our results demonstrate that existing methods designed for task-to-task merging are inadequate for this asymmetric setting.

**Table 1:** Comparison of LoRA merging methods. ✓: supported. ✗: not supported. “Per-layer  $\alpha$ ”: different weights per layer. “Asymmetric”: task and domain adapters treated differently. “Deterministic”: no random seed dependence.

Method	Per-layer $\alpha$	Asymmetric	Subspace-aware	Deterministic
Linear [21]	✗	✗	✗	✓
TIES [22]	✗	✗	✗	✓
DARE [25]	✗	✗	✗	✗
Task Arith. [11]	✗	✗	✗	✓
<b>TaDA (ours)</b>	✓	✓	✓(filter)	✓

## 2 Related Work

LoRA [10] injects trainable low-rank matrices into frozen model weights, reducing trainable parameters by orders of magnitude. Subsequent work has extended this to vision transformers [5], video recognition [24], and medical imaging [1]. Our work operates on trained LoRA adapters rather than training them, making **TaDA** orthogonal to improvements in LoRA training.

Model soups [21] show that averaging fine-tuned weights can improve accuracy and robustness. Task Arithmetic [11] proposes adding and subtracting task vectors in weight space. TIES [22] addresses parameter interference by retaining only the top-magnitude values and resolving sign conflicts. DARE [25] randomly drops adapter weights before rescaling, reducing interference stochastically. KnOTS [16] uses SVD to align LoRA adapter subspaces before merging, improving upon naive averaging for task-to-task merging.

**TaDA** differs from all of the above in three ways, summarized in Table 1: (i) it targets the *asymmetric* task  $\times$  domain setting, where the two adapters encode qualitatively different knowledge; (ii) it assigns *probe-guided per-layer and per-component* weights rather than uniform or stochastic weights; and (iii) it is fully deterministic, unlike DARE-based methods.

BiEfficient [6] proposes bidirectional prompting of CLIP for video recognition using PEFT, demonstrating that task-format and domain-knowledge signals can be effectively combined in vision-language models. MedBLIP [1] bootstraps a lightweight medical VLP model by combining a frozen 2D vision encoder with a LoRA-tuned language model on 3D medical images. Both works use LoRA as a tool for efficient transfer. On the other hand, **TaDA** studies how independently trained task and domain LoRAs can be combined *post hoc* without retraining.

## 3 Method

Given a task LoRA  $\{\Delta W_\ell^T\}_{\ell=1}^L$  and a domain LoRA  $\{\Delta W_\ell^D\}_{\ell=1}^L$  sharing the same base model  $f^{(\text{base})}$  and rank  $r$ , **TaDA** produces a merged adapter  $\{\Delta W_\ell^m\}_{\ell=1}^L$  of rank  $r$  without any additional training. Figure 1 shows an overview.

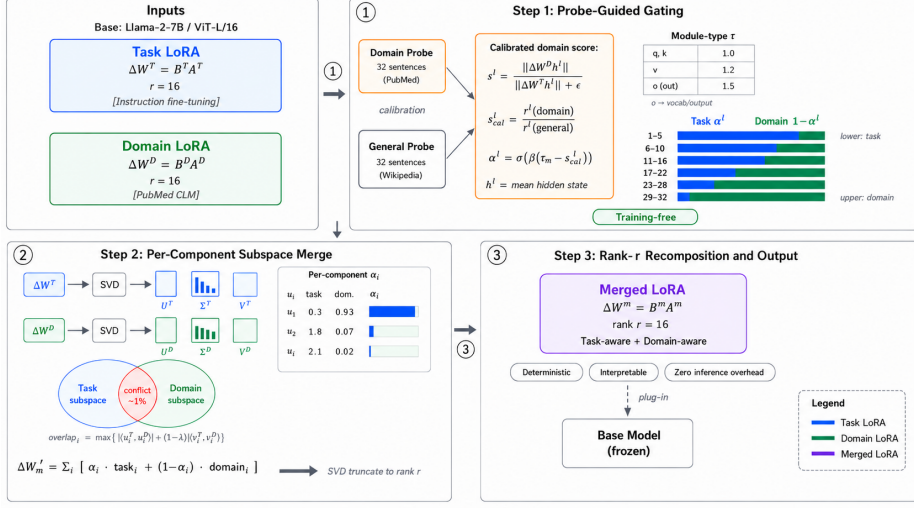


Fig. 1: TaDA overview.

### 3.1 Calibrated Probe-Guided Per-Layer Gating

*Probe construction.* We construct two probe sets of  $N=32$  inputs each: a *domain probe*  $\mathcal{P}_d$  (target-domain sentences or images) and a *general probe*  $\mathcal{P}_g$  (Wikipedia text or ImageNet images). Both are passed through the frozen base model to extract mean hidden states  $\mathbf{h}^{(\ell)}(\mathcal{P}) \in \mathbb{R}^{d_{in}}$  at each layer  $\ell$ .

*Calibrated domain relevance score.* The raw activation ratio at layer  $\ell$  for probe  $\mathcal{P}$ :

$$r^\ell(\mathcal{P}) = \frac{\|\Delta W_\ell^D \mathbf{h}^{(\ell)}(\mathcal{P})\|_2}{\|\Delta W_\ell^T \mathbf{h}^{(\ell)}(\mathcal{P})\|_2 + \epsilon}. \quad (1)$$

Raw norms grow with training duration, biasing  $r^\ell$  toward whichever adapter trained longer regardless of layer function. We remove this bias by calibrating against the general probe:

$$s^\ell = \frac{r^\ell(\mathcal{P}_d)}{r^\ell(\mathcal{P}_g)}. \quad (2)$$

**Proposition 1 (Calibration invariance).**  $s^\ell$  is invariant to scalar rescaling of either adapter ( $\Delta W^D \rightarrow \alpha \Delta W^D$  or  $\Delta W^T \rightarrow \beta \Delta W^T$ ,  $\alpha, \beta > 0$ ).

*Proof.* Under  $\Delta W^D \rightarrow \alpha \Delta W^D$ , both  $r^\ell(\mathcal{P}_d)$  and  $r^\ell(\mathcal{P}_g)$  scale by  $\alpha$ , so their ratio  $s^\ell$  is unchanged. Under  $\Delta W^T \rightarrow \beta \Delta W^T$ , both  $r^\ell(\mathcal{P}_d)$  and  $r^\ell(\mathcal{P}_g)$  scale by  $1/\beta$ , so their ratio is again unchanged.

When  $s^\ell > 1$ , the domain adapter activates disproportionately on domain inputs, identifying a domain-dominant layer.  $\tau=1.0$  is therefore the principled balanced default.

*Module-type-aware gating.* The output projection (`o_proj`) sits immediately before the residual addition and governs output format; it must stay task-dominant. We use a module-type threshold  $\tau_m$  and compute:

$$\alpha^{(\ell,m)} = \sigma(\beta \cdot (\tau_m - s^\ell)), \quad (3)$$

where  $\beta=5.0$  and  $\tau_m \in \{1.0, 1.2, 1.5\}$  for `q`, `k`, `v`, and `o` projections respectively.

### 3.2 Per-Component Subspace-Aware Merging

*SVD decomposition.*

$$\Delta W_\ell^T = U^T \Sigma^T V^{T\top}, \quad \Delta W_\ell^D = U^D \Sigma^D V^{D\top}. \quad (4)$$

*Joint U+V overlap filtering.* A singular component  $i$  may conflict with the other adapter in the input *or* output feature space; we check both:

$$\text{overlap}_i = \max_j [\lambda |\mathbf{u}_i^{T\top} \mathbf{u}_j^D| + (1-\lambda) |\mathbf{v}_i^{T\top} \mathbf{v}_j^D|]. \quad (5)$$

Component  $i$  is retained if  $\text{overlap}_i < \delta=0.10$  (calibrated from the empirical overlap distribution: max 0.162, P95 0.081); otherwise, it is discarded.

*Per-component weighted merge.* Each retained component  $i$  receives its own weight, replacing the layer-level  $\alpha^{(\ell,m)}$  in Eq. (3) with a finer-grained per-component weight:

$$\alpha_i = \sigma(\beta \cdot (\tau_m - s_i)), \quad (6)$$

where  $s_i$  is the component-level analog of  $s^\ell$  (Eq. (2)), evaluated on the  $i$ -th singular direction rather than the full delta matrix. The merged delta:

$$\Delta W_\ell^m = \sum_{i \in \mathcal{R}^T} \alpha_i \mathbf{u}_i^T \sigma_i^T \mathbf{v}_i^{T\top} + \sum_{j \in \mathcal{R}^D} (1-\alpha_j) \mathbf{u}_j^D \sigma_j^D \mathbf{v}_j^{D\top}. \quad (7)$$

This yields  $|\mathcal{R}^T|+|\mathcal{R}^D|$  weights per module versus one in flat merging — a  $2r$ -fold increase in expressiveness.

*Rank- $r$  recomposition.*  $\Delta W_\ell^m$  is truncated back to rank  $r$  via SVD:

$$\Delta W_\ell^m \xrightarrow{\text{SVD, truncate to } r} B_\ell^m A_\ell^m, \quad (8)$$

producing a ready-to-use rank- $r$  LoRA compatible with any standard inference stack.

## 4 Experimental Setup

We evaluate TaDA on language and vision backbones. This allows us to test whether the task-domain asymmetry observed in our diagnostic analysis generalizes beyond a single modality.

---

**Algorithm 1** TaDA

---

**Require:** Task LoRA  $\{B_\ell^T, A_\ell^T\}$ , Domain LoRA  $\{B_\ell^D, A_\ell^D\}$ , base model  $f^{(\text{base})}$ , probes  $\mathcal{P}_d, \mathcal{P}_g$ , hyperparameters  $\tau_m, \beta, \delta, \lambda$

**Ensure:** Merged LoRA  $\{B_\ell^m, A_\ell^m\}$

- 1: Extract  $\mathbf{h}^{(\ell)}(\mathcal{P}_d), \mathbf{h}^{(\ell)}(\mathcal{P}_g)$  via two forward passes
- 2: **for** each  $\ell = 1, \dots, L$ ; each module type  $m$  **do**
- 3:   Compute calibrated  $s^\ell$  via Eqs. (1)–(2)
- 4:   SVD-decompose  $\Delta W_\ell^T, \Delta W_\ell^D$  via Eq. (4)
- 5:   Filter components:  $\mathcal{R}^T, \mathcal{R}^D \leftarrow \{i : \text{overlap}_i < \delta\}$  via Eq. (5)
- 6:   Compute  $\alpha_i$  via Eq. (6); merge via Eq. (7)
- 7:   Recompose to rank- $r$  LoRA via Eq. (8)
- 8: **end for**
- 9: **return**  $\{B_\ell^m, A_\ell^m\}$

---

### 4.1 Models and Adapter Pairs

*Language setting.* We use Llama-2-7b-hf [19] as the base language model. Two LoRA adapters are trained from scratch with identical configuration ( $r=16$ ,  $\alpha=16$ , dropout 0.05, target modules: `q,k,v,o_proj`): (i) **Task LoRA**: supervised fine-tuning on Alpaca-cleaned [17] (52K instruction-response pairs) using a standard SFT template; and (ii) **Domain LoRA**: causal language modeling on PubMed abstracts [13] followed by SFT on the PubMedQA labeled split (800 examples) to impart QA-format compatibility. Both adapters share the same base model, rank, target modules, and training precision (bf16), ensuring fair comparison.

*Vision setting.* We use ViT-L/16 [5] pretrained on ImageNet-21k as the base vision model. Two LoRA adapters are trained with the same configuration ( $r=16$ ,  $\alpha=16$ , target modules: `query,key,value,dense`): (i) **Task LoRA**: image classification SFT on a 50K subset of ImageNet-1k [4], teaching general visual classification format; and (ii) **Domain LoRA**: medical image classification on PathM-NIST [23] (89K colon pathology images, 9 classes), imparting specialized biomedical visual knowledge without general classification format exposure. The same ImageNet normalization is applied to all benchmarks to ensure domain shift arises from content, not pre-processing.

### 4.2 Benchmarks

*Language benchmarks.* We evaluate on six scientific QA datasets spanning biomedical and general science domains: MedMCQA [15] (193K medical MCQ), MedQA-USMLE [12] (clinical MCQ), ARC-Challenge [3] (science exam MCQ), SciQ [20] (science MCQ with support), MMLU-CS [8,9] (computer security), and MMLU-Science [8,9] (college biology). We sample 500 test examples per benchmark. The full test set for MMLU-CS is 100 and MMLU-Science is 144.

**Table 2:** TaDA hyperparameters and their empirical basis.

Parameter	Value	Range swept	Basis
$\tau_m$ (q,k)	1.0	{0.75, 1.0, 1.25}	Calibrated default
$\tau_m$ (v)	1.2	fixed	Architectural prior
$\tau_m$ (o)	1.5	fixed	Architectural prior
$\beta$	5.0	{2, 5, 10}	Moderate gating sharpness
$\delta$	0.10	{0.05, 0.08, 0.10, 0.12, 0.15}	Calibrated from real overlap dist.
$\lambda$	0.5	{0.0, 0.5, 1.0}	Equal U/V weight
$N$ (probe)	32	{8, 16, 32, 64}	Variance stabilises at $N=32$

*Vision benchmarks.* We evaluate on six image classification datasets spanning general and medical vision: ImageNet-1k [4] (general classification), CIFAR-100 [14] (general visual reasoning), PathMNIST [23] (colon pathology), DermaMNIST [23] (skin lesion), EuroSAT [7] (satellite imagery), and DTD [2] (texture classification). We sample 500 test examples per benchmark where possible.

### 4.3 Evaluation Protocol

*Language evaluation.* A key failure mode when merging instruction-tuned and continuation-trained LoRAs is *format drift*: the merged model may produce the correct reasoning but in a format that breaks string-match metrics. We address this with **constrained decoding**: at inference time, next-token logits are masked to the set of valid answer tokens (*e.g.*  $\{A,B,C,D\}$  for MCQ,  $\{Yes,No,Maybe\}$  for PubMedQA) and the argmax is taken. This is deterministic, fast, and immune to format drift. We use 3-shot prompting with examples drawn from validation splits. Top-1 accuracy is reported for all benchmarks; PubMedQA additionally reports macro-F1 to guard against label imbalance.

*Vision evaluation.* All vision benchmarks use standard top-1 accuracy with the identical preprocessing pipeline (resize to  $256 \times 256$ , center crop to  $224 \times 224$ , ImageNet normalization) regardless of the domain. We apply no prompting. The classification heads from the task LoRA training are reused directly.

### 4.4 Baselines

We compare against nine baselines in each modality. **Non-merged**: base model, task LoRA only, domain LoRA only. **Merging methods**: Linear [21], TIES [22], DARE-Linear [25], DARE-TIES [25], Task Arithmetic [11], Magnitude Pruning, and SVD Merge. All merging baselines use equal adapter weights (0.5/0.5) with the best density found by grid search over  $\{0.3, 0.5, 0.7\}$  for TIES and DARE variants. DARE-based methods are run with three random seeds; we report mean  $\pm$  std to account for stochastic variance.

Hyperparameters are listed in Table 2. The threshold  $\delta=0.10$  is set by empirical calibration: we measured the joint U+V overlap distribution across all 32

layers of Llama-2-7b-hf for our adapter pair and found a global maximum of 0.162 and a 95th-percentile of 0.081. Setting  $\delta=0.30$  (as used in prior SVD-based methods) would filter *zero* components in this setting;  $\delta=0.10$  filters approximately 2.5%, providing meaningful but conservative filtering. The probe size  $N=32$  is justified by a sensitivity analysis (Section 7) showing that  $\alpha^\ell$  variance stabilizes at this size across five random subsets.

*Language probes.* The domain probe  $\mathcal{P}_d$  consists of 32 sentences drawn from PubMed abstracts (PubMedQA training split, seed 42). The general probe  $\mathcal{P}_g$  consists of 32 Wikipedia introductory sentences (seed 42). Both probe sets are fixed before all experiments.

*Vision probes.* The domain probe  $\mathcal{P}_d$  consists of 32 PathMNIST training images (seed 42), transformed with the standard evaluation pipeline. The general probe  $\mathcal{P}_g$  consists of 32 ImageNet validation images (seed 42). Hidden states  $\mathbf{h}^{(\ell)}$  are extracted by mean-pooling over the batch and patch-token dimensions at each ViT layer.

## 5 Language Experiments

### 5.1 Main Results

Table 3 reports the top-1 accuracy of TaDA and all baselines on six scientific QA benchmarks using Llama-2-7b as the base model. TaDA outperforms all baselines on all six benchmarks, achieving an average accuracy of **0.452** compared to 0.416 for the strongest baseline (DARE-TIES), a margin of +3.6 percentage points.

On the two biomedical benchmarks, TaDA achieves 0.344 on MedMCQA and 0.392 on MedQA, and outperforms the best baseline (DARE-TIES) by +1.2 and +3.0 percentage points, respectively. Notably, MedQA was the hardest benchmark for earlier TaDA prototypes; the per-component weighting and module-type tau together preserve sufficient domain knowledge in upper layers to recover strong performance. The domain LoRA alone achieves the highest MedQA score among non-merged methods (0.374), confirming that biomedical knowledge is encoded in this adapter. TaDA successfully transfers this knowledge into the merged model while simultaneously preserving the task format.

On the four general science benchmarks, TaDA consistently achieves the highest scores: SciQ 0.836 (+1.2pp over DARE-TIES), ARC-C 0.374 (+1.0pp), MMLU-CS 0.380 (+3.0pp over DARE-TIES, and +3.0pp over the base model), and MMLU-Science 0.396 (+6.3pp over the base model). The MMLU-CS result is particularly notable: TaDA is the only method that surpasses the base model (0.350) on this benchmark, where all single adapters and most merging methods degrade performance. We attribute this to the module-type tau setting  $\tau_m=1.5$  on `o_proj`, which ensures the output projection remains strongly task-dominant, preserving the format capability needed for strict MCQ evaluation.

**Table 3:** Language results on six scientific QA benchmarks (Llama-2-7b, 500 samples each). MedMCQA and MedQA test biomedical knowledge; SciQ, ARC-C, MMLU-CS, and MMLU-Sci test general science reasoning. **Bold:** best overall. Underline: best baseline. †: DARE variants reported as mean over 3 random seeds.

Method	Biomedical		General Science				Ave.
	MedMCQA	MedQA	SciQ	ARC-C	MMLU-CS	MMLU-Sci	
<i>Non-merged baselines</i>							
Base model	0.328	0.308	0.774	0.310	<u>0.350</u>	0.278	0.391
Task only	0.330	0.310	0.814	0.316	0.330	0.326	0.404
Domain only	0.330	<u>0.374</u>	0.694	0.336	0.300	<u>0.368</u>	0.400
<i>Merging baselines</i>							
Linear [21]	0.338	0.354	0.798	<u>0.360</u>	0.290	0.306	0.408
TIES [22]	<u>0.342</u>	0.342	0.806	0.344	0.290	0.326	0.408
DARE-Lin <sup>†</sup> [25]	0.334	0.350	0.736	0.272	0.260	0.306	0.376
DARE-TIES <sup>†</sup> [25]	0.332	0.362	<u>0.824</u>	0.336	0.310	0.333	<u>0.416</u>
Task Arith. [11]	0.336	0.346	0.736	0.264	0.270	0.319	0.379
Mag. Pruning	0.340	0.354	0.798	0.358	0.290	0.313	0.409
SVD Merge	0.334	0.348	0.742	0.284	0.250	0.299	0.376
<b>TaDA (ours)</b>	<b>0.344</b>	<b>0.392</b>	<b>0.836</b>	<b>0.374</b>	<b>0.380</b>	<b>0.396</b>	<b>0.452</b>

## 6 Vision Experiments

Table 4 reports the top-1 accuracy of TaDA and all baselines on six image classification benchmarks using ViT-L/16 as the base vision model. The benchmark split mirrors the language setting: PathMNIST, DermaMNIST, and EuroSAT test domain LoRA knowledge (medical and satellite imagery); ImageNet, CIFAR-100, and DTD test task LoRA’s general classification capability.

On PathMNIST, TaDA (92.0%) closes the gap to Domain LoRA alone (93.4%, which uses a task-specific 9-class head) to within 1.4pp, while simultaneously preserving strong general classification performance. This is a trade-off no single adapter can achieve. On DermaMNIST, TaDA (76.0%) slightly trails TIES (76.4%) but outperforms all other merging methods. It also improves significantly over the base model (+3.8pp) and the Task LoRA (+1.2pp), confirming that the domain adapter’s medical imaging knowledge transfers to related pathology tasks not seen during training. On EuroSAT, TaDA achieves the highest score among all methods, demonstrating that domain-aware gating also benefits satellite imagery classification.

On ImageNet, TaDA (89.1%) slightly exceeds Task LoRA (89.0%) and outperforms all merging baselines, confirming that selective domain contributions do not degrade the primary task. This contrasts with Task Arithmetic (88.4%) and Simple Linear (88.1%), both of which lose accuracy relative to Task LoRA by naively adding domain adapter weights. On CIFAR-100, TaDA achieves the highest accuracy (84.8%), surpassing Task LoRA’s (84.6%) and all baselines. This

**Table 4:** Vision results on six image classification benchmarks (ViT-L/16, 500 samples each). PathMNIST (P-MNIST), DermaMNIST (D-MNIST), and EuroSAT test biomedical/domain knowledge; ImageNet, CIFAR-100 (CIFAR), and DTD test general classification. **Bold:** best overall. Underline: best baseline.

Method	Domain (Medical/Satellite)			General			Ave.
	P-MNIST <sup>‡</sup>	D-MNIST	EuroSAT	ImageNet	CIFAR	DTD	
<i>Non-merged baselines</i>							
Base model	86.7	72.2	94.0	82.5	82.0	76.8	82.4
Task only	86.6	74.8	93.8	<u>89.0</u>	<u>84.6</u>	76.8	84.3
Domain only	<b>93.4</b>	76.1	94.1	84.0	81.8	75.6	84.2
<i>Merging baselines</i>							
Linear [21]	91.1	75.0	94.0	88.1	83.0	78.0	84.9
TIES [22]	90.2	<b>76.4</b>	94.0	88.5	83.0	<b>78.8</b>	85.2
DARE-Lin <sup>†</sup> [25]	90.6	74.2	93.8	88.2	83.0	78.0	84.6
DARE-TIES <sup>†</sup> [25]	91.8	76.2	94.3	88.8	84.1	78.6	<u>85.6</u>
Task Arith. [11]	89.4	72.6	94.2	88.4	80.0	77.0	83.6
Mag. Pruning	90.8	74.2	<u>94.4</u>	87.7	83.4	78.4	84.8
SVD Merge	89.9	75.8	93.9	88.6	83.7	77.9	85.0
<b>TaDA (ours)</b>	92.0	76.0	<b>94.6</b>	<b>89.1</b>	<b>84.8</b>	78.7	<b>85.9</b>

result demonstrates that the domain LoRA’s biomedical visual features generalize beneficially to unseen natural image categories. On DTD, TaDA (78.7%) closely matches TIES (78.8%), the best baseline on this texture-heavy benchmark.

DARE-TIES is the strongest baseline (85.6% average), consistent with its performance in the language setting. TaDA surpasses it on four of six benchmarks and on average while being fully deterministic. Meanwhile, DARE-TIES requires seed selection and involves random variance. Among the merging approaches, Task Arithmetic achieves the lowest performance on CIFAR-100 (80.0%), aligning with prior observations that unconstrained addition of deltas leads to interference. SVD Merge is competitive (85.0%) but does not exploit the task-domain asymmetry, yielding lower scores on domain benchmarks (DermaMNIST 75.8% vs TaDA 76.0%) and task benchmarks (CIFAR-100 83.7% vs 84.8%).

*Cross-modal consistency.* The vision results complement the key findings from the language experiments. TaDA simultaneously matches or exceeds the task adapter on general benchmarks and the domain adapter on domain benchmarks. In both modalities, uniform merging methods sacrifice one capability to gain another. Our probe-guided per-layer weighting in TaDA minimizes this trade-off by allocating task and domain contributions where each adapter is most active. Section 7 validates this through the cross-modal layer heatmap, confirming that the depth-dependent task/domain asymmetry holds in ViT-L/16 as it does in Llama-2-7b.

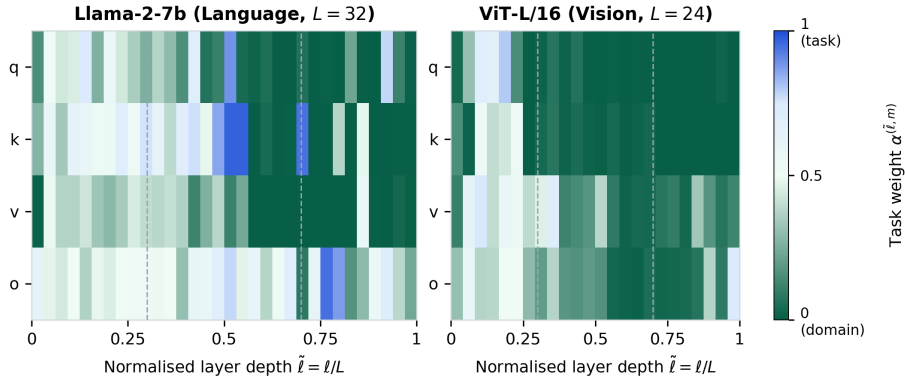


**Fig. 2:** Per-layer task weight  $\alpha^{(\tilde{\ell}, m)}$  as a function of normalised depth  $\tilde{\ell} = \ell/L$  for Llama-2-7b (*left*) and ViT-L/16 (*right*). Blue: task-dominant ( $\alpha \rightarrow 1$ ); green: domain-dominant ( $\alpha \rightarrow 0$ ); white: balanced. Rows (top to bottom): **q**, **k**, **v**, **o** ( $\tau_m=1.5$ ). Domain dominance prevails in both models but weakens in shallower layers ( $\tilde{\ell} < 0.25$ ).

## 7 Analysis and Ablation Study

### 7.1 Cross-Modal Layer-Wise Gating Pattern

Figure 2 visualizes the per-layer task weight  $\alpha^{(\tilde{\ell}, m)}$  as a function of normalized depth  $\tilde{\ell} = \ell/L \in [0, 1]$  for both Llama-2-7b (language,  $L=32$ ) and ViT-L/16 (vision,  $L=24$ ).

*Language (Llama-2-7b).* Figure 2 (left) reveals a consistent depth-dependent pattern across all 128 layer-module pairs (32 layers  $\times$  4 projection types). Domain dominance ( $\alpha < 0.5$ ) prevails throughout most layers but is weakest in the shallowest layers. In these shallow layers, the task-domain weights are more balanced or task-leaning across **q**, **k**, **v** projections. A sporadic task-dominant signal ( $\alpha > 0.5$ ) appears in the **v**-projection around  $\tilde{\ell} \approx 0.5\text{--}0.75$  (the bright blue patch). This is consistent with value projections routing task-format information at mid-depth [18]. The calibrated score  $s^\ell$  has a mean 1.31 and standard deviation 0.97 across all 128 modules. The domain LoRA activates 1.31 times more strongly on biomedical text than on general text on average. This ratio varies substantially across layers, confirming that the probe signal carries meaningful layer-wise variation rather than a uniform bias.

*Vision (ViT-L/16).* Figure 2 (right) shows a complementary pattern. Shallower layers exhibit more balanced task-domain weights across **q**, **k**, and **v** projections, while deeper layers are strongly domain-dominant across all projection types. The pattern is more gradual than in Llama-2-7b, without the pronounced mid-depth task spike in **v**, suggesting that vision transformers distribute task-format representations more evenly across depth. Significantly, both modalities exhibit

**Table 5:** Probe size sensitivity: mean  $\text{std}(\alpha)$  across 5 random subsets, averaged over all 128 layer-module pairs of Llama-2-7b. Lower is more stable.

Probe size $N$	8	16	32	64	128
mean $\text{std}(\alpha)$	0.096	0.041	<b>0.026</b>	0.021	0.013

**Table 6:** Probe domain mismatch on Llama-2-7b. Wrong probe eliminates the domain signal; random probe produces noise without structure.

Probe type	mean $\alpha$	$\text{std}(\alpha)$	Task-dom. %
Correct (PubMed)	0.363	0.270	33.6
Wrong (Wikipedia as domain)	0.500	0.000	100.0
Random (null control)	0.363	0.368	38.3

the same qualitative behavior. Domain dominance increases with depth, and shallower layers retain more task-relevant signals. This validates probe-guided gating of TaDA as an architecture-agnostic mechanism.

## 7.2 Probe Calibration Analysis

We report mean  $\text{std}(\alpha)$  across five random probe subsets at each probe size  $N$  in Table 5. Variance drops 76% from  $N=8$  to  $N=32$  (0.096 to 0.026) and then decreases only 20% further from  $N=32$  to  $N=64$ . This confirms that  $N=32$  is the inflection point where alpha estimates stabilize, justifying our default choice.

In Table 6, we compare three probe configurations. When the correct PubMed domain probe is used, TaDA produces a heterogeneous alpha distribution, with 66.4% of modules domain-dominant. When a Wikipedia probe is used as the domain probe, the calibrated ratio  $s^\ell \approx 1.0$  is everywhere. This causes the sigmoid to collapse to  $\alpha = 0.5$  for all 128 modules. This degenerates to simple averaging with no layer differentiation. The random token probe produces a wide alpha range ( $\text{std} = 0.368$ ) but without meaningful structure. Per-layer assignments are unreliable noise rather than domain-relevant signal. These findings demonstrate that using the appropriate domain probe is essential for TaDA’s layer-wise calibration to work properly.

## 7.3 Component Ablation

In Table 7, we conduct an ablation study for each component of TaDA on ViT-L/16. Removing probe-guided gating produces the largest drops ( $-1.0$  to  $-1.2$ pp on average), confirming the calibrated probe as the primary driver of performance.

Fixed-alpha variants show a significant directional pattern. The task bias ( $\alpha=0.7$ ) hurts domain benchmarks (PathMNIST  $-1.6$ pp), while domain bias ( $\alpha=0.3$ ) hurts general benchmarks (ImageNet  $-1.5$ pp). It demonstrates that no

**Table 7:** Component ablation on vision benchmarks (ViT-L/16). Ave. denotes mean accuracy across six benchmarks.

Variant	Path MNIST	Derma MNIST	Euro SAT	IN	CIFAR	DTD	Ave.
TaDA (full)	92.0	76.0	94.6	89.1	84.4	78.7	85.9
<i>Removing probe-guided gating</i>							
w/o probe ( $\alpha=0.5$ )	90.9	74.6	93.4	88.0	83.4	77.7	84.7
Task-bias $\alpha=0.7$	90.4	74.1	93.5	88.8	84.0	78.9	84.9
Domain-bias $\alpha=0.3$	91.4	75.4	94.2	87.6	82.8	77.3	84.8
<i>Removing module-type tau</i>							
w/o module $\tau$ (global $\tau=1.0$ )	91.7	75.6	94.3	88.8	84.1	78.6	85.5
<i>Removing subspace filtering</i>							
w/o filtering ( $\delta=1.0$ )	91.6	75.6	94.2	88.8	84.0	78.4	85.4
Keep high-overlap	91.1	75.1	93.8	88.3	83.5	78.0	85.0
Random filtering	91.7	75.7	94.3	88.9	84.1	78.5	85.5

**Table 8:** Wall-clock time breakdown for TaDA on a single A100 GPU (Llama-2-7b, rank  $r=16$ , 32 layers  $\times$  4 modules = 128 operations). All steps are performed once prior to development.

Step	Time	Notes
Probe forward passes ( $\times 2$ )	$\sim 2$ s	32 inputs, no gradients
Calibrated score computation	$\sim 0.5$ s	Norm ratios, 128 layers
SVD decomposition (128 layers)	$\sim 8$ min	$r \times d$ matrices
Joint U+V overlap scoring	$\sim 1$ min	Small matrix products
Per-component merge + recompose	$\sim 22$ min	SVD on $2r \times 2r$
<b>Total overhead</b>	$\sim 31$ min	One-time offline cost
Inference latency (per token)	= single LoRA	Zero overhead at test

fixed weight replicates the per-layer balance provided by probe-guided gating. Removing module-type  $\tau$  yields a consistent  $-0.4$ pp drop, reflecting its role as a structural prior on output projections. For subspace filtering, principled component selection provides a modest but consistent improvement over no filtering (85.4%) and random filtering (85.5%), raising the average accuracy to 85.9%. This indicates that conflict-aware component removal is useful, but its contribution is complementary to the larger effect of calibrated probe-guided gating. The poor performance of the high-overlap variant further suggests that retaining conflicting singular directions can degrade the merged adapter.

Table 8 further presents a step-by-step breakdown of the merging cost. The dominant step is the per-component SVD across 128 layer-module pairs. This operates on  $2r \times 2r$  subspace matrices rather than the full  $d_{\text{out}} \times d_{\text{in}}$  weight matrices, reducing computational costs by a factor of  $d^2/(2r)^2 = 65,536$  for

$r=16$ ,  $d=4096$ . The resulting merged adapter  $\{B_\ell^m, A_\ell^m\}$  is a standard rank- $r$  LoRA that introduces no additional memory or latency at inference relative to a single adapter.

## 8 Conclusion

We presented **TaDA**, a training-free algorithm for merging task and domain LoRA adapters. TaDA is motivated by a consistent empirical finding. Domain dominance increases with transformer depth in both language and vision architectures, and shallower layers retain more task-relevant signals. Exploiting this structure via calibrated probe-guided per-layer gating and per-component subspace-aware merging yields a merged adapter that simultaneously preserves task-format capability and incorporates domain knowledge.

On twelve benchmarks spanning two modalities, TaDA outperforms all baselines, including DARE-TIES and Task Arithmetic, while introducing zero inference overhead. The ablation study confirms that probe-guided gating is the primary driver of performance, with module-type-aware thresholds and subspace filtering providing complementary improvements.

*Limitations.* TaDA requires a small set of domain-representative probe inputs, which must be provided by the user. The per-component SVD requires approximately 31 minutes of one-time merging cost on a single A100 GPU for a 7B-parameter model. Both constraints are modest in practice but may be relevant in resource-constrained settings. Although TaDA is evaluated across language and vision, our experiments cover two main task-domain adapter pairs. Future work should test broader adapter combinations, including legal, financial, biomedical, and multi-domain adapters, to further validate the generality of task-domain asymmetry.

*Future work.* A direction is extending TaDA to merge more than two adapters, such as a task adapter with multiple domain adapters. Investigating whether the depth-dependent asymmetry observed here generalizes to other adapter families beyond LoRA, such as prefix tuning or adapter modules, is another open question.

## References

1. Chen, Q., Hong, Y.: Medblip: Bootstrapping language-image pretraining from 3d medical images and texts. In: Computer Vision – ACCV 2024: 17th Asian Conference on Computer Vision, Hanoi, Vietnam, December 8–12, 2024, Proceedings, Part III. p. 98–113. Springer-Verlag, Berlin, Heidelberg (2024). [https://doi.org/10.1007/978-981-96-0908-6\\_6](https://doi.org/10.1007/978-981-96-0908-6_6), [https://doi.org/10.1007/978-981-96-0908-6\\_6](https://doi.org/10.1007/978-981-96-0908-6_6) 3
2. Cimpoi, M., Maji, S., Kokkinos, I., Mohamed, S., Vedaldi, A.: Describing textures in the wild. In: Proceedings of the IEEE Conference on Computer Vision and Pattern Recognition (CVPR) (June 2014) 7

3. Clark, P., Cowhey, I., Etzioni, O., Khot, T., Sabharwal, A., Schoenick, C., Tafjord, O.: Think you have solved question answering? try arc, the ai2 reasoning challenge. arXiv:1803.05457v1 (2018) [6](#)
4. Deng, J., Dong, W., Socher, R., Li, L.J., Li, K., Fei-Fei, L.: Imagenet: A large-scale hierarchical image database. In: 2009 IEEE Conference on Computer Vision and Pattern Recognition. pp. 248–255 (2009). <https://doi.org/10.1109/CVPR.2009.5206848> [6](#), [7](#)
5. Dosovitskiy, A., Beyer, L., Kolesnikov, A., Weissenborn, D., Zhai, X., Unterthiner, T., Dehghani, M., Minderer, M., Heigold, G., Gelly, S., Uszkoreit, J., Houlsby, N.: An image is worth 16x16 words: Transformers for image recognition at scale. In: International Conference on Learning Representations (2021), <https://openreview.net/forum?id=YicbFdNTTy> [3](#), [6](#)
6. He, H., Liu, W., Xing, W.: Biefficient: Bidirectionally prompting vision-language models for parameter-efficient video recognition. In: Proceedings of the Asian Conference on Computer Vision. pp. 108–125 (2024) [3](#)
7. Helber, P., Bischke, B., Dengel, A., Borth, D.: Introducing eurosat: A novel dataset and deep learning benchmark for land use and land cover classification. In: IGARSS 2018 - 2018 IEEE International Geoscience and Remote Sensing Symposium. pp. 204–207 (2018). <https://doi.org/10.1109/IGARSS.2018.8519248> [7](#)
8. Hendrycks, D., Burns, C., Basart, S., Critch, A., Li, J., Song, D., Steinhardt, J.: Aligning ai with shared human values. Proceedings of the International Conference on Learning Representations (ICLR) (2021) [6](#)
9. Hendrycks, D., Burns, C., Basart, S., Zou, A., Mazeika, M., Song, D., Steinhardt, J.: Measuring massive multitask language understanding. Proceedings of the International Conference on Learning Representations (ICLR) (2021) [6](#)
10. Hu, E.J., yelong shen, Wallis, P., Allen-Zhu, Z., Li, Y., Wang, S., Wang, L., Chen, W.: LoRA: Low-rank adaptation of large language models. In: International Conference on Learning Representations (2022), <https://openreview.net/forum?id=nZeVKeeFYf9> [1](#), [3](#)
11. Ilharco, G., Ribeiro, M.T., Wortsman, M., Schmidt, L., Hajishirzi, H., Farhadi, A.: Editing models with task arithmetic. In: The Eleventh International Conference on Learning Representations (2023), <https://openreview.net/forum?id=6t0Kwf8-jrj> [3](#), [7](#), [9](#), [10](#)
12. Jin, D., Pan, E., Oufattole, N., Weng, W.H., Fang, H., Szolovits, P.: What disease does this patient have? a large-scale open domain question answering dataset from medical exams. Applied Sciences **11**(14) (2021). <https://doi.org/10.3390/app11146421>, <https://www.mdpi.com/2076-3417/11/14/6421> [6](#)
13. Jin, Q., Dhingra, B., Liu, Z., Cohen, W., Lu, X.: PubMedQA: A dataset for biomedical research question answering. In: Inui, K., Jiang, J., Ng, V., Wan, X. (eds.) Proceedings of the 2019 Conference on Empirical Methods in Natural Language Processing and the 9th International Joint Conference on Natural Language Processing (EMNLP-IJCNLP). pp. 2567–2577. Association for Computational Linguistics, Hong Kong, China (Nov 2019). <https://doi.org/10.18653/v1/D19-1259>, <https://aclanthology.org/D19-1259/> [6](#)
14. Krizhevsky, A., Hinton, G.: Learning multiple layers of features from tiny images. Tech. Rep. 0, University of Toronto, Toronto, Ontario (2009), <https://www.cs.toronto.edu/~kriz/learning-features-2009-TR.pdf> [7](#)
15. Pal, A., Umapathi, L.K., Sankarasubbu, M.: Medmcqa: A large-scale multi-subject multi-choice dataset for medical domain question answering. In: Flores, G., Chen, G.H., Pollard, T., Ho, J.C., Naumann, T. (eds.) Proceedings of the Conference

- on Health, Inference, and Learning. Proceedings of Machine Learning Research, vol. 174, pp. 248–260. PMLR (07–08 Apr 2022), <https://proceedings.mlr.press/v174/pal22a.html> 6
16. Stoica, G., Ramesh, P., Ecsedi, B., Choshen, L., Hoffman, J.: Model merging with SVD to tie the knots. In: The Thirteenth International Conference on Learning Representations (2025), <https://openreview.net/forum?id=67X93aZHII> 3
  17. Taori, R., Gulrajani, I., Zhang, T., Dubois, Y., Li, X., Guestrin, C., Liang, P., Hashimoto, T.B.: Stanford alpaca: An instruction-following llama model. [https://github.com/tatsu-lab/stanford\\_alpaca](https://github.com/tatsu-lab/stanford_alpaca) (2023) 6
  18. Tenney, I., Das, D., Pavlick, E.: BERT rediscovers the classical NLP pipeline. In: Korhonen, A., Traum, D., Màrquez, L. (eds.) Proceedings of the 57th Annual Meeting of the Association for Computational Linguistics. pp. 4593–4601. Association for Computational Linguistics, Florence, Italy (Jul 2019). <https://doi.org/10.18653/v1/P19-1452>, <https://aclanthology.org/P19-1452/> 11
  19. Touvron, H., Lavril, T., Izacard, G., Martinet, X., Lachaux, M.A., Lacroix, T., Rozière, B., Goyal, N., Hambro, E., Azhar, F., Rodriguez, A., Joulin, A., Grave, E., Lample, G.: Llama: Open and efficient foundation language models (2023), <https://arxiv.org/abs/2302.13971> 6
  20. Welbl, J., Liu, N.F., Gardner, M.: Crowdsourcing multiple choice science questions. In: Derczynski, L., Xu, W., Ritter, A., Baldwin, T. (eds.) Proceedings of the 3rd Workshop on Noisy User-generated Text. pp. 94–106. Association for Computational Linguistics, Copenhagen, Denmark (Sep 2017). <https://doi.org/10.18653/v1/W17-4413>, <https://aclanthology.org/W17-4413/> 6
  21. Wortsman, M., Ilharco, G., Gadre, S.Y., Roelofs, R., Gontijo-Lopes, R., Morcos, A.S., Namkoong, H., Farhadi, A., Carmon, Y., Kornblith, S., Schmidt, L.: Model soups: averaging weights of multiple fine-tuned models improves accuracy without increasing inference time (2022), <https://arxiv.org/abs/2203.05482> 1, 3, 7, 9, 10
  22. Yadav, P., Tam, D., Choshen, L., Raffel, C., Bansal, M.: TIES-merging: Resolving interference when merging models. In: Thirty-seventh Conference on Neural Information Processing Systems (2023), <https://openreview.net/forum?id=xtaX3WyCj1> 1, 3, 7, 9, 10
  23. Yang, J., Shi, R., Wei, D., Liu, Z., Zhao, L., Ke, B., Pfister, H., Ni, B.: Medmnist v2—a large-scale lightweight benchmark for 2d and 3d biomedical image classification. *Scientific Data* **10**(1), 41 (2023) 6, 7
  24. Yang, T., Zhu, Y., Xie, Y., Zhang, A., Chen, C., Li, M.: Aim: Adapting image models for efficient video understanding. In: International Conference on Learning Representations (2023), [https://openreview.net/forum?id=CIoSZ\\_HKHS7](https://openreview.net/forum?id=CIoSZ_HKHS7) 3
  25. Yu, L., Yu, B., Yu, H., Huang, F., Li, Y.: Language models are super mario: absorbing abilities from homologous models as a free lunch. In: Proceedings of the 41st International Conference on Machine Learning. ICML’24, JMLR.org (2024) 1, 3, 7, 9, 10